Phase Diagram, Design of Monolayer Binary Colloidal Crystals, and Their Fabrication Based on Ethanol-Assisted Self-Assembly at the Air/Water Interface

Zhengfei Dai, Yue Li,* Guotao Duan, Lichao Jia, and Weiping Cai*

Key Lab of Materials Physics, Anhui Key Lab of Nanomaterials and Nanotechnology, Institute of Solid State Physics, Chinese Academy of Sciences, Hefei 230031, People's Republic of China

ABSTRACT Flexible structural design and accurate controlled fabrication with structural tunability according to need for binary or multicomponent colloidal crystals have been expected. However, it is still a challenge. In this work, the phase diagram of monolayer binary colloidal crystals (bCCs) is established on the assumption that both large and small polystyrene (PS) colloidal spheres can stay at the air/water interface, and the range diagram for the size ratio and number ratio of small to large colloidal spheres is presented. From this phase diagram, combining the range diagram, we can design and relatively accurately control fabrication of the bCCs with specific structures (or patterns) according to need, including single or mixed patterns with the given relative content. Further, a simple and facile approach is presented to fabricate large-area (more than 10 cm^2) monolayer bCCs without any surfactants, using differently sized PS spheres, based on ethanol-assisted self-assembly at the air/water interface. bCCs with different patterns and stoichiometries are thus designed from the established phase diagram and then successfully fabricated based on the volume ratios ($V_{S/L}$) of the small to large PS suspensions using the presented colloidal self-assembling method. Interestingly, these monolayer bCCs can be transferred to any desired substrates using water as the medium. This study allows us to design desired patterns of monolayer bCCs and to more accurately control their structures with the used $V_{S/L}$.

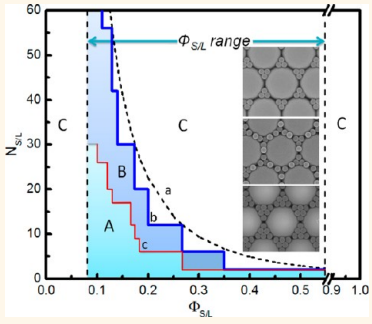

KEYWORDS: phase diagram · pattern design · monolayer binary colloidal crystals · ethanol-assisted self-assembly · air/water interface

In the past decade, colloidal crystals with a two-dimensional (2D) or three-dimensional (3D) ordered arrangement of monodispersed colloidal spheres have attracted much attention because of their potential far-ranging applications in a variety of fields, such as photonics,[1−3] microelectronic mechanical systems,[4] catalysis,[5,6] lithography,[7−10] surface-enhanced Raman scattering (SERS),[11−13] sensors,[14,15] and superhydrophobic surfaces.[16−18] So far, most of the research has mainly focused on fabrication of colloidal crystals composed of single-diameter colloidal spheres *via* diversified routes.[19−21] These colloidal crystals have some limitations in structural controllability and hence restrict the tunability of their performances.[22,23] Recent studies have indicated that binary colloidal crystals (bCCs), consisting of colloidal spheres with two sizes, could exhibit many more advantages compared to colloidal crystals with single-sized colloidal spheres in some applications, due to the structural diversity. For instance, they can easily realize photonic crystals with a high degree of photonic band-gap tunability[24,25] and can also be used as templates for ordered porous films with flexibly controlled structures.[26−28] Additionally, they are suitable for crystallographic model research,[29,30] *etc.*

Up to now, bCCs have been usually obtained by a self-assembly approach, using a mixture of colloidal spheres with two sizes. Their structures are primarily determined by the size ratio of large (L) to small (S) colloidal spheres as well as the relative content of both spheres.[31,32] Many different self-assembly routes have been developed for 2D or 3D bCCs over the past years. For instance, Ozin *et al.* have produced hexagonally close-packed 2D bCCs with an area of several square centimeters *via* coassembly of binary dispersions of monodispersed microspheres.[33] On the basis of the confined convective assembly method, Park *et al.* have fabricated 2D bCCs with various superlattices, especially new and more complicated LS_4 and LS_5 structures.[34,35] Here, LS_N denotes the number ratio N of small to large spheres in a bCC, which characterizes the pattern of bCCs. Jia *et al.* have successfully

* Address correspondence to yueli@issp.ac.cn, wpcai@issp.ac.cn.

Received for review March 24, 2012 and accepted July 30, 2012.

Published online July 30, 2012
10.1021/nn3013178

synthesized 2D bCCs with different structures *via* layer-by-layer colloidal templates and one-step spin-coating, respectively.[26,28] Van Blaaderen *et al*. have reported a simple layer-by-layer process to grow well-ordered 3D bCCs with stoichiometries of LS_1, LS_2, and LS_3.[32] Wang *et al*. have employed a stepwise spin-coating process to fabricate 3D bCCs with LS_2 and LS_3 structures by manipulating the size ratio and the spin speed.[36] *Via* a direct co-deposition method, 3D bCCs and inverse opals, with different patterns and long-range ordering, were also fabricated.[5] Additionally, there are many other methods for 2D or 3D bCCs, such as stepwise dip-coating,[37] contact printing,[38] electric-field-induced assembly,[39] horizontal deposition,[40,41] and area-confinement evaporation-induced assembly.[42] Generally, these approaches are time-consuming or have difficulty providing uniform and well-controlled bCCs with large dimensions. In a mixed suspension with colloidal spheres of two sizes, sedimentation of large spheres is usually faster than small ones. So it is difficult to get large-scale bCCs by general self-assembly methods, especially for 2D bCCs, which can be used to fabricate some high-quality 3D ones with controllable layer number *via* a layer-by-layer process.[43,44] Hence, controlling the fabrication of 2D bCCs, with large dimensions and a homogeneous and well-defined structure, by a simple and flexible route is still expected.

Recently, self-assembly of colloidal spheres at the air/water interface has been developed as a promising high-throughput approach for fabrication of large-area 2D colloidal crystals.[43,45,46] In this method, by injecting the colloidal suspension into water, the colloidal spheres spread on the water surface in minutes, and then a monolayer colloidal crystal is formed on the water surface (or the air/water interface), where the spheres can stay and freely move. Here, the water surface functions like a substrate that allows for the spheres' movement and arrangement more easily than other solid substrates. However, both the large and small colloidal spheres will not remain on the water surface without using surfactants, such as sodium dodecyl sulfate.[23,45,47,48] In addition, it is still a challenge to design and fabricate 2D bCCs with controllable patterns or structures according to need based on the self-assembly at the air/water interface.

Obviously, if large and small colloidal spheres can stay on the water surface, monolayer (or 2D) bCCs can be obtained by air/water interfacial self-assembly. For polystyrene (PS) colloidal spheres, the density is slightly higher than water. It seems that it is impossible for PS spheres to stay at the air/water interface when the PS sphere suspension is injected into the water just *via* the resultant force of PS sphere gravity and the buoyancy of water. However, recently, we have found that if we dropped the aqueous PS sphere suspensions, containing some volatile alcohol or methanol, into the water film, the PS spheres can be kept on the water surface (see the Results and Discussion section). Here, on the assumption that both large and small colloidal spheres can stay on the surface of water, we try to establish the phase diagram of monolayer bCCs, from which we can design and fabricate monolayer or 2D bCCs with controllable and specific structures (or patterns) according to need, including single or mixed patterns with the given relative content. Further, a simple and facile approach is presented to fabricate large-area (more than 10 cm^2) monolayer bCCs without any surfactants, using differently sized monodispersed PS spheres, based on ethanol-assisted self-assembly at the air/water interface. The 2D bCCs with different patterns and stoichiometries are thus designed from the established phase diagram and successfully fabricated just by the volume ratios of the small to large PS sphere suspensions. Our method needs neither special equipment, such as spin-coating and vertical lifting devices, nor any surfactants. Importantly, these bCCs can be transferred to any needed substrates, using water as medium. The transferability of the bCCs could be applied to many fields to obtain different devices with special performances, such as photonics, sensors, and solar cells. The details are reported in this article.

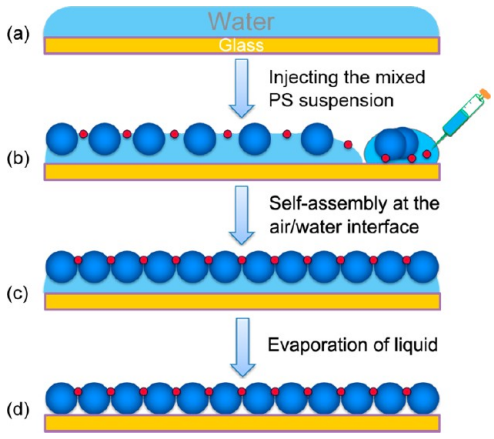

Scheme 1. Schematic illustration for the fabrication strategy of monolayer binary colloidal crystals.[a]

[a] (a) A well-cleaned glass slide with water film is placed horizontally. (b) Large and small PS spheres stay on the water film. (c) Monolayer binary colloidal crystal is formed on the air/water interface after self-assembly. (d) Monolayer binary colloidal crystal is on the slide after evaporation of liquid.

DESIGN AND PHASE DIAGRAM OF MONOLAYER BCCS

Strategy. On the basis of the assumption that both large and small colloidal microspheres can stay at the air/water interface, microspheres can self-assemble and form monolayer bCCs at the air/water interface. We thus present a synthesis strategy, as shown in Scheme 1. First, a cleaned glass slide is placed on a flat table. Deionized water is dropped onto it to form a water film with a thickness of 2 mm (Scheme 1a). Then, a specific amount of well-mixed aqueous suspensions

with large and small PS spheres, containing alcohol (water *vs* alcohol, 1:1 in volume), is continuously slowly injected along the edge of the preformed water film on the slide (Scheme 1b). Meanwhile, both small and large PS spheres quickly emerge on the water film's surface and self-assemble into a 2D bCC at the air/water interface (Scheme 1c). Finally, the large-area monolayer bCCs can be formed on the slide after completely evaporating the liquid (Scheme 1d).

Structural Design. In this strategy, monolayer bCCs with different structures or patterns can be designed depending on stoichiometries and the size ratio of PS colloidal spheres. For the monodispersed PS sphere suspensions, the PS spheres' number (n) in unit volume of suspension is given by

$$n = 6w/(\pi QD^3) \quad (1)$$

where w is the PS sphere content (in weight) in unit volume of suspensions (bought from Alfa Aesar Company), and Q and D are the density (1.05 g/cm^3) and the diameter of the PS spheres, respectively. For a bCC with N_S and N_L, which are the numbers of small and large PS spheres, respectively, if using two PS sphere suspensions with different PS sphere sizes, from eq 1, we have

$$\frac{N_S}{N_L} = \frac{V_S n_S}{V_L n_L} = \frac{V_S w_S D_L^3}{V_L w_L D_S^3} \quad (2)$$

where V is the used suspension volume and the subscripts S and L denote the small and large PS spheres, respectively. If letting $N_{S/L} = (N_S/N_L)$, $V_{S/L} = (V_S/V_L)$, and $\Phi_{S/L} = (D_S/D_L)$, eq 2 can also be written as

$$N_{S/L} = \frac{V_{S/L}}{(\Phi_{S/L})^3}\frac{w_S}{w_L} \quad (3)$$

If the different colloidal suspensions contain the same PS sphere content as in this work, or $w_S = w_L$, eq 3 can be simplified to

$$N_{S/L} = \frac{V_{S/L}}{(\Phi_{S/L})^3} \quad (3')$$

Under the assumption that both large and small PS spheres can uniformly disperse and stay at the air/water interface, some special values of $N_{S/L}$ (or the number ratio of small to large spheres) in a monolayer bCC should correspond to not only stoichiometry but also the specific structures or patterns of the bCC. For the polydispersed PS sphere system, Ohara *et al.*'s investigation has indicated that the interparticle interaction between large spheres is stronger than that between small particles.[49] Owing to the strong interaction, the large spheres will be assembled into a hexagonally ordered monolayer and the overall potential energy of the system is minimized when the small spheres are at the periphery of each large sphere.[50] Hence, the surface of the monolayer with

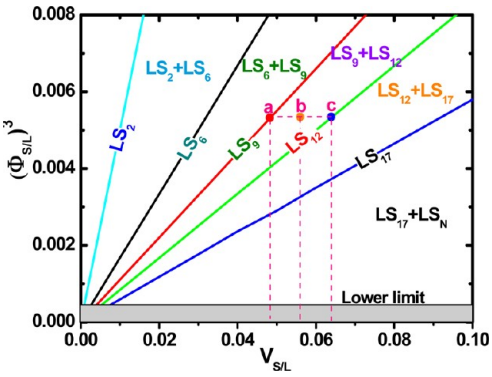

Figure 1. Phase diagram of monolayer bCCs, or $(\Phi_{S/L})^3$, as a function of $V_{S/L}$ for different monolayer LS_N bCCs. Each plot corresponds to the denoted single-phase line. The areas between two adjacent straight lines correspond to the denoted two-phase regions. Shadow area corresponds to a $\Phi_{S/L}$ smaller than the lower limit (or 0.077). The points a, b, and c indicate the LS_9, LS_9–LS_{12} hybrid, and LS_{12} bCCs, respectively.

Chart 1. Geometrical structures for the monolayer binary colloidal crystals with the patterns (a) LS_6, (b) LS_9, (c) LS_{12}, and (d) LS_{17}.

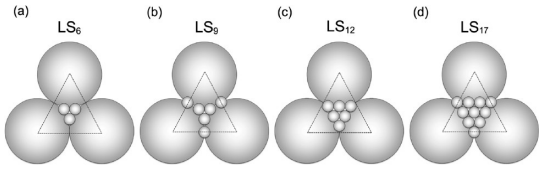

the close-packed large spheres provides two kinds of interstices suitable for the arrangement of small spheres, including the 3-fold voids among three adjoining large spheres and the bridges connecting these 3-fold voids. Further, inspired by crystallography, the stacking of small spheres might in fact be the closest and most energetically favored. Chart 1 schematically shows the monolayer bCCs with the patterns LS_6, LS_9, LS_{12}, and LS_{17}, corresponding to the $N_{S/L}$ values 6, 9, 12, and 17, respectively. The bCCs with simple patterns in Chart 1, such as LS_2, LS_6, and LS_{12}, are based on previous reports.[34] Compared with the bCC pattern LS_6, the pattern LS_9 is formed by one more small sphere located at each bridge on the base of the LS_6 bCC, of which we can see a similar miniature in the literature.[51] Here we design the bCC pattern LS_{17} based on a geometrical configuration at a specific size ratio ($\Phi_{S/L} = 0.175$, see the following sections). The small spheres in the bCC patterns LS_6, LS_{12}, and LS_{17} are all in equilateral triangle forms, which indicate lower potential energies.

Different specific $N_{S/L}$ values correspond to different structures or patterns of 2D bCCs. From eq 3 or 3′, we know that such structures can be quantitatively controlled just by the size ratio ($\Phi_{S/L}$) of the colloidal spheres and the volume ratio ($V_{S/L}$) of the used colloidal suspensions, which is more clearly demonstrated in Figure S1, corresponding to $N_{S/L}$ as a linear function

of $V_{S/L}$ under different $\Phi_{S/L}$ values based on eq 3′. Under a given $\Phi_{S/L}$ value, only some special $V_{S/L}$ values correspond to the bCCs with special patterns, such as LS_6, LS_9, LS_{12}, and LS_{17} (or $N_{S/L}$ = 6, 9, 12, and 17, respectively), as seen in the plot of $\Phi_{S/L}$= 0.175 in Figure S1. This means that the other $V_{S/L}$ values can not induce a monostructured pattern. Furthermore, the bCC's structure is highly sensitive to the $\Phi_{S/L}$ value. A small $\Phi_{S/L}$ value will lead to high slope of the plot $N_{S/L}$ *vs* $V_{S/L}$, indicating difficulty in controlling fabrication by $V_{S/L}$, as seen in Figure S1.

Phase Diagram of Monolayer bCCs. Further, if monolayer bCC with the pattern LS_N is considered as a structural phase, we can establish its phase diagram from eq 3′. In eq 3, there are three variables, $\Phi_{S/L}$, $V_{S/L}$, and $N_{S/L}$. Under constant temperature and pressure, the degrees of freedom (*f*) can be determined to be 2 based on the Gibbs phase rule. The phase diagram can be plotted as $(\Phi_{S/L})^3$ *vs* $V_{S/L}$ from eq 3′ under the given LS_N or some specific $N_{S/L}$ values, as shown in Figure 1. Obviously, when LS_N is fixed (see each straight line in Figure 1), $f = 1$, and thus the phase number must be 1 according to the phase rule. Therefore, the straight lines $(\Phi_{S/L})^3$ *vs* $V_{S/L}$ should correspond to single patterns (or single-phase lines) in this phase diagram. Similarly, the areas between two adjacent straight lines are the two-phase regions, which should consist of the adjacent two patterns (phases). Only when the point $[(\Phi_{S/L})^3, V_{S/L}]$ is on the straight line can the single pattern (or single phase) be obtained. Otherwise, we can obtain only the mixed phases consisting of the adjacent two patterns. The relative content of the two patterns can be determined by the lever rule, depending on $V_{S/L}$ under a given $\Phi_{S/L}$ value. For a given point b in the two-phase region (LS_{N1} +LS_{N2}), as marked in two phase region (LS_9 + LS_{12}) in Figure 1, the relative contents of the adjacent patterns LS_{N1} (point a) and LS_{N2} (point c) can be determined by the ratio of line segments $|ab|$ to $|bc|$ (see Figure 1). This method can also offer an alternative way to design and fabricate some hybrid structures.

This phase diagram gives us an effective way to design the desired patterns of monolayer bCCs and to accurately determine their structures from the used $\Phi_{S/L}$ and $V_{S/L}$. We can also quantitatively control the fabrication of bCCs with a specific pattern, according to the design, just by $\Phi_{S/L}$ and/or $V_{S/L}$, which has been confirmed by our experiments (see the following sections).

Applicability. The establishment of the phase diagram in Figure 1 is based on the assumption that both large and small PS spheres can stay and be well-dispersed at the air/water interface. Otherwise, that mentioned above is not tenable.

Also, the $\Phi_{S/L}$ and $N_{S/L}$ values should be in reasonable ranges for monolayer bCCs. For the size ratio ($\Phi_{S/L}$) of the colloidal spheres, obviously, the small spheres should, at least, be bigger than the size of the interstices

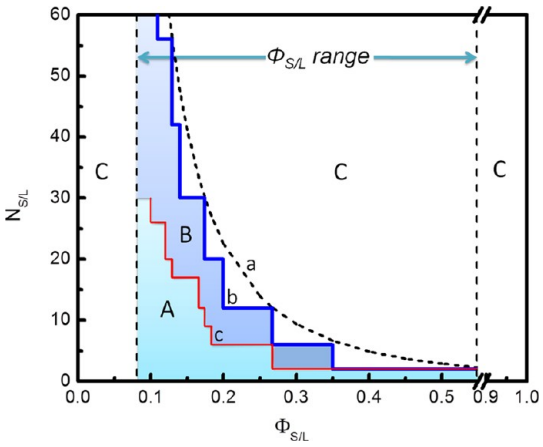

Figure 2. Range diagram of $N_{S/L}$ *vs* $\Phi_{S/L}$. Curves a and b: $N_{S/L(max)}$ as a function of $\Phi_{S/L}$ from eq 4 and eq 4′, respectively. Curve c: $N_{S/L(max)}$ as a function of $\Phi_{S/L}$ after consideration of structural stability.

among the three close-packed large spheres, especially for LS_2 bCC, but cannot be too large. Otherwise, they would influence the self-assembly of large spheres and the structural stability of the monolayer bCCs. $\Phi_{S/L}$ should fall in a range of $(2\sqrt{3} - 3)/6 \le \Phi_{S/L} \le \sqrt{3}/3)$, or $0.077 \le \Phi_{S/L} \le 0.577$, as illustrated in Chart S1a. The details are seen in "Determination of the range for $\Phi_{S/L}$" in the Supporting Information. For instance, for the large sphere with a 2000 nm diameter, the corresponding small spheres' size should be in the range from 154 to 1154 nm for a monolayer bCC with high quality.

For the upper limit of $N_{S/L}$, or $N_{S/L(max)}$, under the assumption of monolayer close-packed arrangement of the small spheres, as geometrically analyzed in Chart S1b, we have

$$N_{S/L(max)} = \left(\frac{1}{\Phi_{S/L}} - \sqrt{3} + 1\right)\left(\frac{1}{\Phi_{S/L}} - \sqrt{3} + 2\right) \quad (4)$$

or $N_{S/L(max)}$ depends on the size ratio $\Phi_{S/L}$, as illustrated in curve a in Figure 2. In fact, the real $N_{S/L(max)}$ should be a step-like function of $\Phi_{S/L}$ due to the integer's requirement of the sphere number, or

$$N_{S/L(max)} = \mathrm{Int}\left(\frac{1}{\Phi_{S/L}} - \sqrt{3} + 1\right)\mathrm{Int}\left(\frac{1}{\Phi_{S/L}} - \sqrt{3} + 2\right) \quad (4')$$

where Int(*x*) is defined as the largest integer less than or equal to *x*. The corresponding results are shown in curve b (fold-line) in Figure 2 (the details are seen in "Determination of the ranges for $N_{S/L}$" in the Supporting Information) and should be smaller than the values of curve a in Figure 2. However, the small spheres should be arranged in a special way due to the structural stability, instead of the normal monolayer close-packed arrangement (Chart S1b), as clearly shown in Chart S2. The details of Chart S2 are seen in the Supporting Information. Briefly, for the binary

colloidal crystals, the packing of spheres is entropically driven and energetically favored. When the size of the large sphere is set, the overall potential energy is mainly determined by the free energy (E) of the small spheres. The E can be divided into two parts: (i) gravity potential energy (E_g); (ii) size-dependent interparticle interaction energy (E_i). According to previous research,[49] for the small spheres, the interaction with the large spheres is much stronger than that with other small spheres. So their interactions with large spheres play an essential role in the E_i of small spheres. A lower free energy of small spheres will result in a more stable arrangement (see "Determination of the ranges for $N_{S/L}$" in the Supporting Information). In this case, $N_{S/L(max)}$ could be lower for better structural stability, as illustrated in curve c in Figure 2. There are three regions in Figure 2. When ($N_{S/L}$, $\Phi_{S/L}$) is in region A, the structure is stable. Meanwhile, the patterns in region B are possible but unstable. In region C, the bCCs are impossible or nonexistent. This means that we can fabricate only the stable monolayer bCCs with the structures or patterns in region A. The diagram shown in Figure 2 provides us clear guidance to design and fabricate monolayer bCCs with stable patterns (structures), combined with the phase diagram in Figure 1.

RESULTS AND DISCUSSIONS

Structure and Morphology. On the basis of the ethanol-assisted self-assembly route shown in Scheme 1, we have synthesized a series of PS sphere monolayer bCCs with different patterns using $\Phi_{S/L}$ = 0.175 (small and large sphere sizes are 350 and 2000 nm, respectively). Typically, Figure 3a presents a photo of the as-prepared sample with a large area (*ca.* 18 cm^2), corresponding to $V_{S/L}$ = 0.048. It displays iridescent color, which originates from diffraction of the sample, indicating formation of a periodic array. Figure 3b gives the typical corresponding FESEM image (a top view). We can see that large spheres (2000 nm) are in a hexagonal close-packed arrangement and small spheres (350 nm) are confined exclusively within the surface grooves induced by the large spheres. Such film is of bCC structure with the pattern LS_9 (see the inset in Figure 3b), close to that shown in Chart 1b. This is in good agreement with the result estimated from eq 3′ or point a in Figure 1. The surface of the monolayer with the close-packed large spheres provides two kinds of interstices suitable for the arrangement of small spheres, including the 3-fold voids (or site 1) among three adjoining large spheres and the bridges (or site 2) connecting these 3-fold voids, as marked in the inset of Figure 3b. Further, the side-view examination has shown that there is no small PS sphere situated on the substrate (slide), as shown in Figure 3c. In addition, the large and small PS spheres are all in monolayer forms, respectively. This indicates that both the large and small PS spheres indeed stay and uniformly disperse at the air/water interface during self-assembly.

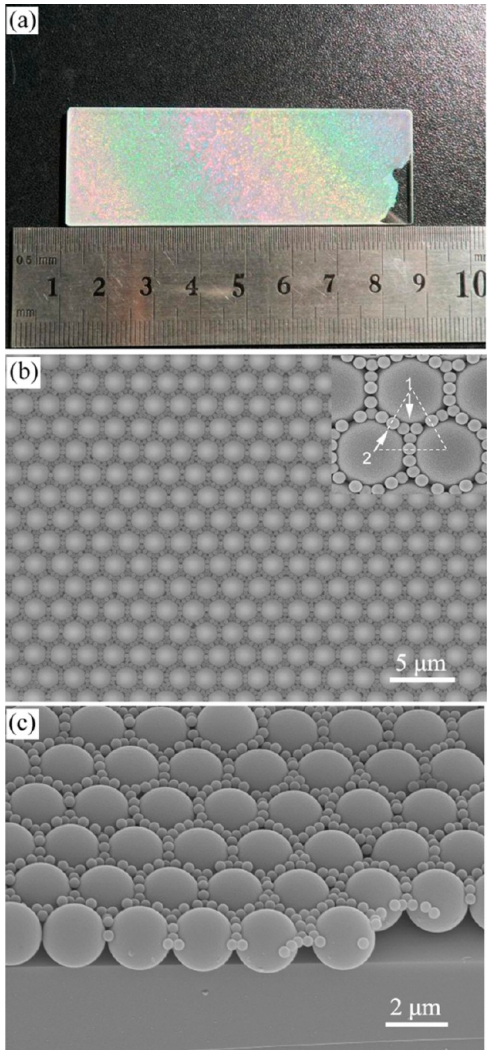

Figure 3. Morphology for the binary colloidal crystal prepared by the ethanol-assisted self-assembly route shown in Scheme 1 ($\Phi_{S/L}$ = 0.175, $V_{S/L}$ = 0.048). (a) Photo of the sample on a glass slide, showing iridescent color. (b and c) Corresponding top view and side view of FESEM images, respectively. Inset: Local magnified image of (b), showing LS_9 pattern.

Further, we have also checked the structural uniformity of the colloidal crystals in the whole sample, showing good uniformity, as typically shown in Figure S2, corresponding to nine different regions in the sample. The whole sample is uniform in structure. Here it should mentioned that there exists a small amount (*ca.* 5%) of LS_{12} or LS_6 phase as well as the voids, in addition to the dominant (~95%) bCC phase LS_9 due to the experimental precision. This small amount of mixed phases is mainly attributed to local fluctuation of $V_{S/L}$ induced by imprecise component ratio and/or a local insufficient dispersion of large and small spheres at the air/water interface (see the following subsection).

Tunability and Controllability of the bCC Patterns. On basis of the phase diagram in Figure 1, we can obtain

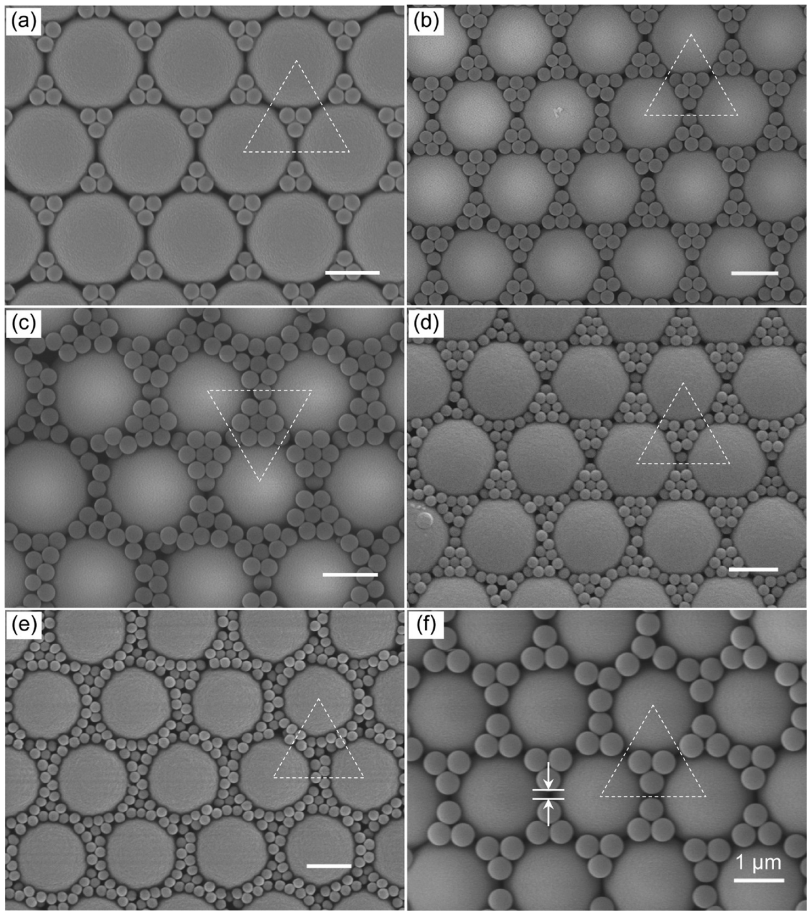

Figure 4. FESEM images of bCCs with different $\Phi_{S/L}$ and $V_{S/L}$ values. (a−c) $\Phi_{S/L}$ = 0.175, $V_{S/L}$ = 0.032, 0.064, and 0.09, respectively. (d and e) $\Phi_{S/L}$ = 0.1, $V_{S/L}$ = 0.02 and 0.027, respectively. (f) $\Phi_{S/L}$= 0.25, $V_{S/L}$ = 0.094. All scale bars are 1 μm.

monolayer bCCs with specific patterns just by controlling the volume ratio ($V_{S/L}$) of the used suspensions with small and large PS spheres. For the patterns or the phases such as LS_6, LS_{12}, and LS_{17}, under a given $\Phi_{S/L}$ = 0.175 or $(\Phi_{S/L})^3$ = 0.00536 (say, 350/2000 nm), from eq 3′ or the phase diagram in Figure 1, the corresponding $V_{S/L}$ should be 0.032, 0.064, and 0.091, respectively. These are all in good agreement with the experimental results, as illustrated in Figure 4a−c. Obviously, with an increase of $V_{S/L}$, the small PS spheres locate in turn according to the patterns shown in Chart 1. In other words, the small spheres preferentially situate at 3-fold voids (site 1) among three close-packed large spheres and then the bridges (site 2) spanning these 3-fold voids rather than flow freely, which is easy to be understood due to the different energies at different sites.[52] According to eq 4′, for the PS sphere size ratio 350/2000 or $\Phi_{S/L}$ = 0.175, $N_{S/L(max)}$ is 20 (see curve b in Figure 2), which is not stable in structure. The corresponding $N_{S/L(max)}$ value with stable structure should be 17, as seen in curve c in Figure 2. Hence, under $\Phi_{S/L}$ = 0.175, the pattern LS_{17} shown in Figure 4c is the most complicated pattern with stable structure for monolayer bCCs.

Similarly, for the other $\Phi_{S/L}$ values, we can also control fabrication of the monolayer bCCs with specific patterns, according to the phase diagram in Figure 1. Figure 4d and e show the monolayer bCCs corresponding to $V_{S/L}$ values of 0.020 and 0.026, respectively, under $\Phi_{S/L}$ = 0.1 (or 200/2000 nm in this work), which is close to its lower limit. The single phase with the structures LS_{20} and LS_{26} is obtained. This is also in agreement with the predictions by eq 3′. Further, if we use a large size ratio of PS spheres, say, $\Phi_{S/L}$ = 0.25, according to eq 4′, the upper limit of $N_{S/L}$ is 12 (see curve b in Figure 2). But the $N_{S/L(max)}$ value with stable structure should be 6 (see curve c in Figure 2), corresponding to the LS_6 pattern. From eq 3′, we can determine the $V_{S/L}$ to be 0.094 for the LS_6 pattern. This is also well consistent with the experimental result, as shown in Figure 4f. In addition, we can see that the spacing between the three close-packed small spheres (see the double-headed arrows in Figure 4f) is smaller than the small sphere's size. So, LS_6 is the most complicated pattern with stable structure for $\Phi_{S/L}$ = 0.25, in accordance with that shown in curve c in Figure 2.

If the $V_{S/L}$ values are between two adjoining specific values, a monolayer bCC with mixed patterns (phases) tends to form. Figure 5a shows the typical result corresponding to $V_{S/L}$ = 0.056, which is between

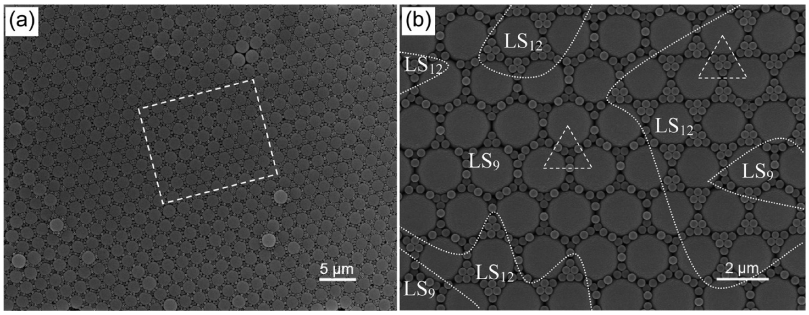

Figure 5. FESEM images of the monolayer bCC prepared from $\Phi_{S/L} = 0.175$ and $V_{S/L} = 0.056$. (a) Image with low magnification. (b) Enlarged view corresponding to the area marked in (a), showing coexistence of the patterns LS_9 and LS_{12} with boundaries (the dashed lines).

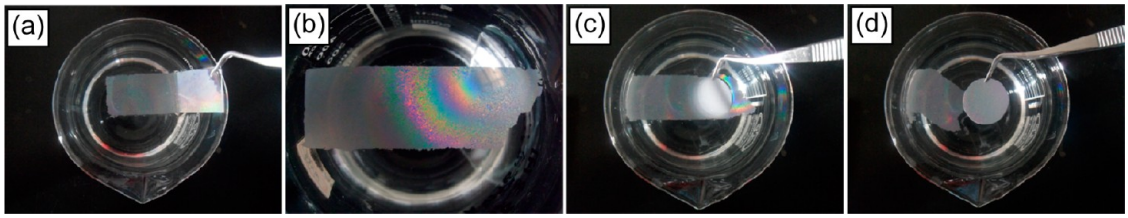

Figure 6. Photographs of monolayer bCC transferring from one substrate to the others. (a) The monolayer bCC on a slide is slantwise immersed into the distilled water in a beaker. (b) The bCC film is integrally lifted off from its substrate (slide) and floats on the surface of the water. (c) The bCC is picked up by a Si substrate. (d) The bCC is transferred onto the Si substrate.

0.048 and 0.064 under $\Phi_{S/L} = 0.175$ (see point b in Figure 1), exhibiting the mixed structure consisting of two phases, LS_9 and LS_{12}, with phase interfacial lines between them (see the dashed lines in Figure 5b), as predicted in the phase diagram in Figure 1. No other pattern is observed. It is also reasonable from the viewpoint of the energy during the self-assembly. At this $V_{S/L}$ value, the energy should be minimal for the mixed structure with LS_9 and LS_{12} patterns induced by local stoichiometric fluctuation during self-assembly. Also, the relative contents of the phase LS_9 or LS_{12} can be determined to be 50% by the lever rule, which exhibits a good coincidence with our observation (see Figure 5). This method can also offer an alternative way to design and fabricate some hybrid structures.

In summary, based on the phase diagram in Figure 1, combining the applicable range diagram of $N_{S/L}$ *vs* $\Phi_{S/L}$ in Figure 2, we can design and accurately control the fabrication of large-sized monolayer bCCs with specific structural patterns according to our needs. In addition to some previously reported bCC phases, here, we have, for the first time, obtained the bCC phases LS_{17}, LS_{20}, and LS_{26} and the LS_9–LS_{12} hybrid phases.

Transferability and Defects of bCCs. Importantly, if we slantwise immerse the monolayer bCCs on the slide into the distilled water in a beaker, such monolayer can be integrally lifted off from its substrate (slide) and stay on surface of the water and can thus be transferred to any other desired substrates (*e.g.*, silicon substrates, ITO substrates) just by picking it up with the new substrates we need, as demonstrated in Figure 6. This transferability is very useful since it can provide the possibility to fabricate bCC-based devices on any substrates we need. Also, 3D bCCs can be fabricated by a layer-by-layer strategy based on the transferable route shown in Figure 6.

It should be pointed out that the quality of the as-synthesized monolayer bCCs is associated with the operation conditions. There sometimes exist some defects, such as vacancies, splits, and structural nonuniformity in the as-synthesized monolayer bCCs, depending on the carefulness of one's operation and experimental precision. There always exist a few vacancies (about 10^{-4} in proportion) of the large PS spheres in the hexagonally close-packed layer even with careful operating, as representatively shown in Figure 7a, corresponding to one vacancy in the local area of the monolayer bCC with LS_9 pattern [or Figure S2(e), (g)]. It is worth mentioning that there is no small PS sphere within this pit. It is different from the structure fabricated by Ozin *et al.*[33] using the dip-coating method, where there are several small spheres within the vacancy sites. If the glass slide is not well cleaned or insufficiently hydrophilic, line-like defects or splits will be formed in the monolayer bCCs, as illustrated in Figure 7b. Formation of such a split could be attributed to the water evaporation-induced shrinkage of the bCC film and adhesion of large PS spheres on the insufficiently hydrophilic slide.

In addition, sufficient mix of the small and large PS sphere suspensions before injection into water is also crucial for the formation of high-quality monolayer bCCs. Otherwise, the small and large PS spheres will

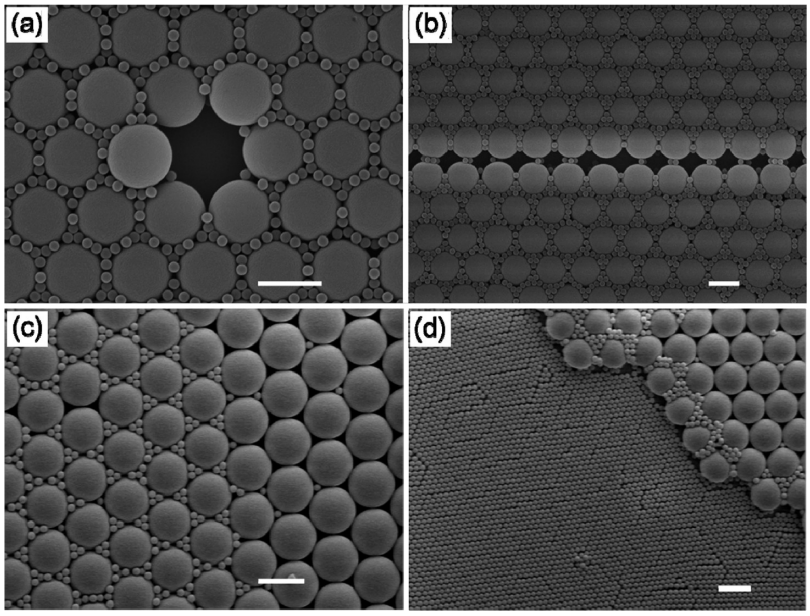

Figure 7. FESEM images of some typical defects in monolayer bCCs. (a) Vacancy site in a LS_9 bCC. (b) Linear split in a LS_{12} bCC. (c and d) Structural nonuniformity due to segregation of the small and large PS spheres during self-assembly. All scale bars are 2 μm.

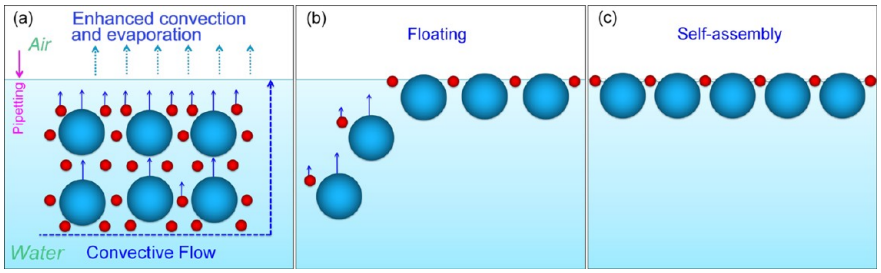

Figure 8. Schematic illustration of monolayer bCC formation (the details are given in the text). (a) The PS spheres are immersed into the solvent (water) driven by gravity. (b) The PS spheres ascend and stay on the water surface. (c) The PS spheres are self-organized into a bCC on the air/water interface.

segregate during self-assembly, leading to structural nonuniformity, as shown in Figure 7c,d. Normally, the number of such defects is largely decreased as long as we sufficiently disperse or mix the PS sphere suspensions and use well-cleaned or sufficiently hydrophilic slides. In this case, from the phase diagram in Figure 1, combining the range diagram of $N_{S/L}$ *vs* $\Phi_{S/L}$ in Figure 2, we can obtain monolayer bCCs with the desired patterns.

Formation of Monolayer bCCs. In the system of colloid suspensions, due to the slight density difference between the PS colloidal spheres and the water, the moving behavior of the colloidal spheres is not dominated by their gravity, although they are slightly denser than water. They mainly exhibit Brownian motion. However, they can be affected by other factors, such as evaporation and convection of solvents. For instance, the convection of solvent is strongly enhanced by rapid evaporation of the volatile ethanol or methanol mixed in the colloidal suspension, and the colloidal spheres can thus be easily transferred to the solvent surface along the direction of convection. Once these colloidal spheres reach the solvent surface, they will be trapped or stay on the air/solvent interface, according to the self-assembling rule, as previously reported.[53−55]

In our work, when the mixture of the PS sphere suspension and ethanol (1:1 in volume) is injected into the water film, the PS spheres will first be immersed into the solvent (water), as schematically illustrated in Figure 8a. Subsequently, the injected ethanol can diffuse due to its concentration gradient and quickly evaporate from the water surface, leading to enhanced convective flow in the solvent. The PS spheres with large or small size can thus be transported onto the water surface under such convective flow of solvents. Once the PS spheres reach the water surface, they will be trapped at the water/air interface due to the PS sphere surface's dewetting effect caused by the hydrophobicity,[7] and they will not sink again due to their density being very close to that of water and the high surface tension (Figure 8b). The PS spheres, staying on the water surface, will assemble into colloidal crystals

by the water capillary force caused by the meniscus among the PS spheres.[54,56] If large and small PS spheres, with enough size difference, are sufficiently mixed with each other and uniformly dispersed on the water surface, large PS spheres can self-organize into a hexagonal close-packed arrangement and the small spheres will uniformly fill the upper interstices among the close-packed large spheres (Figure 8c). Obviously, the small PS spheres tend to a regular geometric arrangement in the interstices among the close-packed large PS spheres due to energy minimization. Finally, the monolayer bCCs can be obtained in the interface of air/water or on the substrate after complete evaporation of the water (see Figure 6). Also, if the large and small PS spheres are insufficiently mixed or the glass substrate was not cleaned, we can only produce bCCs with defects (Figure 7).

Additionally, according to Shimmin *et al.*'s previous research,[53] if neither diffusion nor convection of the solvent can disperse the PS microspheres' accumulation, a colloidal crystal with a multilayer is expected to form. In our work, the convection is strongly enhanced by ethanol evaporation and the diffusion of PS particles along the convection direction is improved owing to the very low particle volume fraction (0.025%) in solvent; so a colloidal monolayer is preferably formed rather than a multilayer at the air/liquid interface.

CONCLUSION

In summary, both large and small PS spheres can stay on the surface of water by dropping a mixture of PS sphere suspensions with alcohol into the water. On this basis, we have established a phase diagram of the monolayer bCCs and presented a range diagram of $N_{S/L}$ *vs* $\Phi_{S/L}$. From such a phase diagram, combined with the range diagram, we have designed monolayer bCCs with controllable and specific structures (or patterns), including single or mixed patterns with a given relative content. Further, a simple and facile approach has been presented to fabricate large-area (more than 10 cm^2) monolayer bCCs without any surfactants, using differently sized monodispersed PS spheres, based on ethanol-assisted self-assembly at the air/water interface. bCCs with different patterns and stoichiometries are thus successfully fabricated according to the design, based on the volume ratios ($V_{S/L}$) of the small to large PS sphere suspensions and the PS spheres' size ratios, $\Phi_{S/L}$. Interestingly, these monolayer bCCs can be transferred to any substrate we need, using water as the medium. This study gives an effective guide to design desired patterns of monolayer bCCs and to accurately determine their structures. We can thus quantitatively control the fabrication of bCCs with specific patterns, according to the design, just by $V_{S/L}$ and/or $\Phi_{S/L}$ values from the phase diagram in Figure 1.

EXPERIMENTAL SECTION

Materials and Methods. Glass slides (7.5 × 2.5 cm^2) with a thickness of 2 mm were washed with acetone, ethanol, and deionized water in an ultrasonic bath and then in turn cleaned in 98% H_2SO_4/H_2O_2 (3:1 in volume), $H_2O/NH_3 \cdot H_2O/H_2O_2$ (5:1:1 in volume), and deionized water, followed by drying with N_2 gas. After this thorough cleaning, the surface of the slides is sufficiently hydrophilic. Monodispersed PS sphere suspensions (200, 350, 500, and 2000 nm in PS sphere diameters) [2.5 wt % in water (or $w_S = w_L$), surfactant-free] were obtained from Alfa Aesar Corporation. The small (350, 200, or 500 nm) and large (2000 nm) PS sphere suspensions were mixed with each other in different suspension volume ratios ($V_{S/L}$) according to eq 3 or eq 3′. The mixed suspensions were subsequently diluted in the same volume of ethanol and ultrasonicated for absolute uniformity. Large-area monolayer bCCs were fabricated according to the strategy shown in Scheme 1. First, we placed a cleaned glass slide on a flat table and dropped deionized water on it to form a water film covering the entire surface of the slide (about 2 mm in thickness). Second, the ethanol-diluted mixed suspension (*ca.* 200 μL in volume) with a specific $V_{S/L}$ value was taken with a micropipet and continuously, slowly injected into the water at the edge of the preformed water film for about 5 min. After injection, we kept it for 5 min for PS sphere self-assembly at the air/water interface. Finally, a large-area monolayer bCC was formed on the slide after liquid evaporation by using a gentle airflow at 30 °C. It should be mentioned that when we directly inject the mixed PS sphere suspensions without dilution by ethanol, the PS spheres cannot self-assemble at the air/water interface.

The morphologies of the samples were examined on a field-emission scanning electron microscope (FESEM, Sirion 200). The optical photographs of the large-area 2D bCCs on the glass slides and the air/water interface were obtained using a digital camera (Samsung L110).

Conflict of Interest: The authors declare no competing financial interest.

Acknowledgment. The authors acknowledge the financial support from the National Basic Research Program of China (Grant No. 2012CB932303), Recruitment Program of Global Experts (C), Natural Science Foundation of China (Grant Nos. 50831005, 51002158, 10974203), Anhui Provincial Natural Science Foundation (Grant No. 11040606M62), and Anhui Provincial Natural Science Foundation for Distinguished Young Scholar (Grant No. 1108085J20).

Supporting Information Available: Characterization of the sample uniformity; determination of the range for $\Phi_{S/L}$; determination of the ranges for $N_{S/L}$. This material is available free of charge *via* the Internet at http://pubs.acs.org.

Note Added after ASAP Publication: Due to a production error, the graphic of Scheme 1 was missing from the PDF version published August 6, 2012. The corrected paper was reposted August 10, 2012.

REFERENCES AND NOTES

1. Vlasov, Y. A.; Bo, X.-Z.; Sturm, J. C.; Norris, D. J. On-Chip Natural Assembly of Silicon Photonic Bandgap Crystals. *Nature* **2001**, *414*, 289–293.
2. Wang, J. J.; Li, Q.; Knoll, W.; Jonas, U. Preparation of Multilayered Trimodal Colloid Crystals and Binary Inverse Opals. *J. Am. Chem. Soc.* **2006**, *128*, 15606–15607.
3. Duan, G.; Cai, W.; Luo, Y.; Sun, F. A Hierarchically Structured $Ni(OH)_2$ Monolayer Hollow-Sphere Array and Its Tunable Optical Properties over a Large Region. *Adv. Funct. Mater.* **2007**, *17*, 644–650.
4. Choi, S.; Park, I.; Hao, Z.; Holman, H. Y. N.; Pisano, A. P.; Zohdi, T. I. Ultrafast Self-Assembly of Microscale Particles by Open-Channel Flow. *Langmuir* **2010**, *26*, 4661–4667.
5. Wang, J.; Ahl, S.; Li, Q.; Kreiter, M.; Neumann, T.; Burkert, K.; Knoll, W.; Jonas, U. Structural and Optical Characterization

of 3D Binary Colloidal Crystal and Inverse Opal Films Prepared by Direct Co-Deposition. *J. Mater. Chem.* **2008**, *18*, 981–988.
6. Zhao, S.; Zhao, J.; Lou, L. L.; Liu, S. X. Amino-Functionalized SBA-15 Immobilized $NiBr_2(PPh_3)_2$ as a Highly Effective Catalyst for ATRP of MMA. *Microporous Mesoporous Mater.* **2011**, *137*, 36–42.
7. Burmeister, F.; Schafle, C.; Keilhofer, B.; Bechinger, C.; Boneberg, J.; Leiderer, P. From Mesoscopic to Nanoscopic Surface Structures: Lithography with Colloid Monolayers. *Adv. Mater.* **1998**, *10*, 495–497.
8. Hulteen, J. C.; Treichel, D. A.; Smith, M. T.; Duval, M. L.; Jensen, T. R.; Van Duyne, R. P. Nanosphere Lithography: Size-Tunable Silver Nanoparticle and Surface Cluster Arrays. *J. Phys. Chem. B* **1999**, *103*, 3854–3863.
9. Li, Y.; Lee, E. J.; Cai, W.; Kim, K. Y.; Cho, S. O. Unconventional Method for Morphology-Controlled Carbonaceous Nanoarrays Based on Electron Irradiation of a Polystyrene Colloidal Monolayer. *ACS Nano* **2008**, *2*, 1108–1112.
10. Duan, G. T.; Cai, W. P.; Luo, Y. Y.; Lv, F. J.; Yang, J. L.; Li, Y. Design and Electrochemical Fabrication of Gold Binary Ordered Micro/Nanostructured Porous Arrays *via* Step-by-Step Colloidal Lithography. *Langmuir* **2009**, *25*, 2558–2562.
11. Kelly, K. L.; Coronado, E.; Zhao, L. L.; Schatz, G. C. The Optical Properties of Metal Nanoparticles: The Influence of Size, Shape, and Dielectric Environment. *J. Phys. Chem. B* **2003**, *107*, 668–677.
12. Duan, G. T.; Cai, W. P.; Luo, Y. Y.; Li, Z. G.; Li, Y. Electrochemically Induced Flowerlike Gold Nanoarchitectures and Their Strong Surface-Enhanced Raman Scattering Effect. *Appl. Phys. Lett.* **2006**, *89*, 211905.
13. Liu, G. Q.; Cai, W. P.; Kong, L. C.; Duan, G. T.; Lu, F. J. Vertically Cross-Linking Silver Nanoplate Arrays with Controllable Density Based on Seed-Assisted Electrochemical Growth and Their Structurally Enhanced SERS Activity. *J. Mater. Chem.* **2010**, *20*, 767–772.
14. Sun, F. Q.; Cai, W. P.; Li, Y.; Jia, L. C.; Lu, F. Direct Growth of Mono- and Multilayer Nanostructured Porous Films on Curved Surfaces and Their Application as Gas Sensors. *Adv. Mater.* **2005**, *17*, 2872–2877.
15. Waitz, T.; Wagner, T.; Sauerwald, T.; Kohl, C. D.; Tiemann, M. Ordered Mesoporous In_2O_3: Synthesis by Structure Replication and Application as a Methane Gas Sensor. *Adv. Funct. Mater.* **2009**, *19*, 653–661.
16. Li, Y.; Huang, X. J.; Heo, S. H.; Li, C. C.; Choi, Y. K.; Cai, W. P.; Cho, S. O. Superhydrophobic Bionic Surfaces with Hierarchical Microsphere/SWCNT Composite Arrays. *Langmuir* **2007**, *23*, 2169–2174.
17. Shiu, J. Y.; Kuo, C. W.; Chen, P. L.; Mou, C. Y. Fabrication of Tunable Superhydrophobic Surfaces by Nanosphere Lithography. *Chem. Mater.* **2004**, *16*, 561–564.
18. Yang, H. T.; Jiang, P. Scalable Fabrication of Superhydrophobic Hierarchical Colloidal Arrays. *J. Colloid Interface Sci.* **2010**, *352*, 558–565.
19. Yang, S. M.; Jang, S. G.; Choi, D. G.; Kim, S.; Yu, H. K. Nanomachining by Colloidal Lithography. *Small* **2006**, *2*, 458–475.
20. Patoka, P.; Giersig, M. Self-Assembly of Latex Particles for the Creation of Nanostructures with Tunable Plasmonic Properties. *J. Mater. Chem.* **2011**, *21*, 16783–16796.
21. Li, Y.; Koshizaki, N.; Cai, W. P. Periodic One-Dimensional Nanostructured Arrays Based on Colloidal Templates, Applications, and Devices. *Coord. Chem. Rev.* **2011**, *255*, 357–373.
22. Li, Y.; Cai, W.; Duan, G. Ordered Micro/nanostructured Arrays Based on the Monolayer Colloidal Crystals. *Chem. Mater.* **2008**, *20*, 615–624.
23. Zhou, Z. C.; Yan, Q. F.; Li, Q.; Zhao, X. S. Fabrication of Binary Colloidal Crystals and Non-Close-Packed Structures by a Sequential Self-Assembly Method. *Langmuir* **2007**, *23*, 1473–1477.
24. Meseguer, F. Colloidal Crystals as Photonic Crystals. *Colloids Surf., A* **2005**, *270*−*271*, 1–7.
25. Hynninen, A. P.; Thijssen, J. H. J.; Vermolen, E. C. M.; Dijkstra, M.; Van Blaaderen, A. Self-Assembly Route for Photonic Crystals with a Bandgap in the Visible Region. *Nat. Mater.* **2007**, *6*, 202–205.
26. Jia, L. C.; Cai, W. P. Micro/Nanostructured Ordered Porous Films and Their Structurally Induced Control of the Gas Sensing Performances. *Adv. Funct. Mater.* **2010**, *20*, 3765–3773.
27. Jia, L. C.; Cai, W. P.; Wang, H. Q. Layer-by-Layer strategy for the General Synthesis of 2D Ordered Micro/Nanostructured Porous Arrays: Structural, Morphological and Compositional Controllability. *J. Mater. Chem.* **2009**, *19*, 7301–7307.
28. Jia, L. C.; Cai, W. P.; Wang, H. Q.; Sun, F. Q.; Li, Y. Hetero-apertured Micro/Nanostructured Ordered Porous Array: Layer-by-Layered Construction and Structure-Induced Sensing Parameter Controllability. *ACS Nano* **2009**, *3*, 2697–2705.
29. Leunissen, M. E.; Christova, C. G.; Hynninen, A. P.; Royall, C. P.; Campbell, A. I.; Imhof, A.; Dijkstra, M.; van Roij, R.; van Blaaderen, A. Ionic Colloidal Crystals of Oppositely Charged Particles. *Nature* **2005**, *437*, 235–240.
30. Vermolen, E. C. M.; Kuijk, A.; Filion, L. C.; Hermes, M.; Thijssen, J. H. J.; Dijkstra, M.; van Blaaderen, A. Fabrication of Large Binary Colloidal Crystals with a NaCl Structure. *Proc. Natl. Acad. Sci. U. S. A.* **2009**, *106*, 16063–16067.
31. Tommaseo, G.; Petekidis, G.; Steffen, W.; Fytas, G.; Schofield, A. B.; Stefanou, N. Hypersonic Acoustic Excitations in Binary Colloidal Crystals: Big *versus* Small Hard Sphere Control. *J. Chem. Phys.* **2007**, 126.
32. Velikov, K. P.; Christova, C. G.; Dullens, R. P. A.; van Blaaderen, A. Layer-by-Layer Growth of Binary Colloidal Crystals. *Science* **2002**, *296*, 106–109.
33. Kitaev, V.; Ozin, G. A. Self-Assembled Surface Patterns of Binary Colloidal Crystals. *Adv. Mater.* **2003**, *15*, 75–78.
34. Kim, M. H.; Im, S. H.; Park, O. O. Fabrication and Structural Analysis of Binary Colloidal Crystals with Two-Dimensional Superlattices. *Adv. Mater.* **2005**, *17*, 2501–2505.
35. Choi, H. K.; Kim, M. H.; Im, S. H.; Park, O. O. Fabrication of Ordered Nanostructured Arrays Using Poly(dimethylsiloxane) Replica Molds Based on Three-Dimensional Colloidal Crystals. *Adv. Funct. Mater.* **2009**, *19*, 1594–1600.
36. Wang, D. Y.; Mohwald, H. Rapid Fabrication of Binary Colloidal Crystals by Stepwise Spin-Coating. *Adv. Mater.* **2004**, *16*, 244–247.
37. Zhang, G.; Wang, D. Y.; Gu, Z. Z.; Mohwald, H. Fabrication of Superhydrophobic Surfaces from Binary Colloidal Assembly. *Langmuir* **2005**, *21*, 9143–9148.
38. Burkert, K.; Neumann, T.; Wang, J. J.; Jonas, U.; Knoll, W.; Ottleben, H. Automated Preparation Method for Colloidal Crystal Arrays of Monodisperse and Binary Colloid Mixtures by Contact Printing with a Pintool Plotter. *Langmuir* **2007**, *23*, 3478–3484.
39. Huang, X. G.; Zhou, J.; Fu, M.; Li, B.; Wang, Y. H.; Zhao, Q.; Yang, Z. W.; Xie, Q.; Li, L. T. Binary Colloidal Crystals with a Wide Range of Size Ratios *via* Template-Assisted Electric-Field-Induced Assembly. *Langmuir* **2007**, *23*, 8695–8698.
40. Wang, L. K.; Wan, Y.; Li, Y. Q.; Cai, Z. Y.; Li, H. L.; Zhao, X. S.; Li, Q. Binary Colloidal Crystals Fabricated with a Horizontal Deposition Method. *Langmuir* **2009**, *25*, 6753–6759.
41. Liu, J.; Cai, Y.; Deng, Y. H.; Sun, Z. K.; Gu, D.; Tu, B.; Zhao, D. Y. Magnetic 3-D Ordered Macroporous Silica Templated from Binary Colloidal Crystals and Its Application for Effective Removal of Microcystin. *Microporous Mesoporous Mater.* **2010**, *130*, 26–31.
42. Singh, G.; Pillai, S.; Arpanaei, A.; Kingshott, P. Layer-by-Layer Growth of Multicomponent Colloidal Crystals over Large Areas. *Adv. Funct. Mater.* **2011**, *21*, 2556–2563.
43. Retsch, M.; Zhou, Z. C.; Rivera, S.; Kappl, M.; Zhao, X. S.; Jonas, U.; Li, Q. Fabrication of Large-Area, Transferable Colloidal Monolayers Utilizing Self-Assembly at the Air/Water Interface. *Macromol. Chem. Phys.* **2009**, *210*, 230–241.
44. Zhang, J. H.; Li, Y. F.; Zhang, X. M.; Yang, B. Colloidal Self-Assembly Meets Nanofabrication: From Two-Dimensional Colloidal Crystals to Nanostructure Arrays. *Adv. Mater.* **2010**, *22*, 4249–4269.
45. Yu, J.; Yan, Q.; Shen, D. Co-Self-Assembly of Binary Colloidal Crystals at the Air−Water Interface. *ACS Appl. Mater. Interfaces* **2010**, *2*, 1922–1926.

46. Vogel, N.; de Viguerie, L.; Jonas, U.; Weiss, C. K.; Landfester, K. Wafer-Scale Fabrication of Ordered Binary Colloidal Monolayers with Adjustable Stoichiometries. *Adv. Funct. Mater.* **2011**, *21*, 3064–3073.
47. Bardosova, M.; Pemble, M. E.; Povey, I. M.; Tredgold, R. H. The Langmuir-Blodgett Approach to Making Colloidal Photonic Crystals from Silica Spheres. *Adv. Mater.* **2010**, *22*, 3104–3124.
48. Cong, H. L.; Cao, W. X. Array Patterns of Binary Colloidal Crystals. *J. Phys. Chem. B* **2005**, *109*, 1695–1698.
49. Ohara, P. C.; Leff, D. V.; Heath, J. R.; Gelbart, W. M. Crystallization of Opals from Polydisperse Nanoparticles. *Phys. Rev. Lett.* **1995**, *75*, 3466–3469.
50. Bishop, K. J. M.; Wilmer, C. E.; Soh, S.; Grzybowski, B. A. Nanoscale Forces and Their Uses in Self-Assembly. *Small* **2009**, *5*, 1600–1630.
51. Singh, G.; Pillai, S.; Arpanaei, A.; Kingshott, P. Highly Ordered Mixed Protein Patterns over Large Areas from Self-Assembly of Binary Colloids. *Adv. Mater.* **2011**, *13*, 1519–1523.
52. Wang, D. Y.; Mohwald, H. Template-Directed Colloidal Self-Assembly - The Route to 'Top-Down' Nanochemical Engineering. *J. Mater. Chem.* **2004**, *14*, 459–468.
53. Shimmin, R. G.; DiMauro, A. J.; Braun, P. V. Slow Vertical Deposition of Colloidal Crystals: A Langmuir-Blodgett Process? *Langmuir* **2006**, *22*), 6507–6513.
54. Wickman, H. H.; Korley, J. N. Colloid Crystal Self-Organization and Dynamics at the Air/Water Interface. *Nature* **1998**, *393*, 445–447.
55. Im, S. H.; Park, O. O. Effect of Evaporation Temperature on the Quality of Colloidal Crystals at the Water-Air Interface. *Langmuir* **2002**, *18*, 9642–9646.
56. Xia, Y.; Gates, B.; Yin, Y.; Lu, Y. Monodispersed Colloidal Spheres: Old Materials with New Applications. *Adv. Mater.* **2000**, *12*, 693–713.